Life and death in the Chicxulub impact crater: A record of the Paleocene-Eocene Thermal Maximum

Vann Smith[1,2], Sophie Warny[1,2], Kliti Grice[3], Bettina Schaefer[3], Michael T. Whalen[4], Johan Vellekoop[5,6], Elise Chenot[7], Sean P.S. Gulick[8,9], Ignacio Arenillas[10], Jose A. Arz[10], Thorsten Bauersachs[11], Timothy Bralower[12], François Demory[13], Jérôme Gattacceca[13], Heather Jones[12], Johanna Lofi[14], Christopher M. Lowery[8], Joanna Morgan[15], Noelia B. Nuñez Otaño[16], Jennifer M.K. O'Keefe[17], Katherine O'Malley[4], Francisco J. Rodríguez-Tovar[18], Lorenz Schwark[3,11], and the Expedition 364 Scientists

[1]Department of Geology and Geophysics, Louisiana State University, Baton Rouge, LA 70803, USA
[2]Museum of Natural Science, Louisiana State University, Baton Rouge, LA 70803, USA
[3]Western Australian Organic and Isotope Geochemistry Centre, The Institute for Geoscience Research, School of Earth and Planetary Science, Curtin University, Perth, WA 6102, Australia
[4]Department of Geosciences, University of Alaska Fairbanks, Fairbanks, AK 99775, USA
[5]Department of Earth and Environmental Sciences, Division of Geology, KU Leuven, 3001 Heverlee, Belgium
[6]Analytical, Environmental and Geo-Chemistry (AMGC), Vrije Universiteit Brussel, 1050 Brussels, Belgium
[7]GeoRessources, Université de Lorraine, CNRS, 54 500 Vandœuvre-lès-Nancy, France
[8]Department of Geological Sciences, Jackson School of Geosciences, University of Texas at Austin, TX 78712, USA
[9]Institute for Geophysics, Jackson School of Geosciences, University of Texas at Austin, TX 78712, USA
[10]Departamento de Ciencias de la Tierra e Instituto Universitario de Investigación de Ciencias Ambientales de Aragón, Universidad de Zaragoza, Pedro Cerbuna 12, E-50009 Zaragoza, Spain
[11]Department of Organic Geochemistry, Institute of Geosciences, Christian-Albrechts-University, Kiel, 24118, Germany
[12]Department of Geosciences, Pennsylvania State University, University Park, PA 16801, USA
[13]CNRS, Aix-Marseille Univ, IRD, Coll France, INRAE, CEREGE, Aix-en-Provence, France
[14]Géosciences Montpellier, lUniversité Montpellier, CNRS, Montpellier, France
[15]Department of Earth Science and Engineering, Imperial College London, SW7 2AZ, UK
[16]Facultad de Ciencia y Tecnología (FCyT), Universidad Autónoma de Entre Ríos, CONICET, Laboratorio de Geología del Neógeno-Cuaternario, Diamante, Entre Ríos, Argentina
[17]Department of Physics, Earth Science, and Space Systems Engineering, Morehead State University, Morehead, KY, USA
[18]Departamento de Estratigrafía y Paleontología, Facultad de Ciencias, Universidad de Granada, 18002 Granada, Spain

Correspondence to: Vann Smith (vannpaleo@gmail.com)

Abstract. Thermal stress on the biosphere during the extreme warmth of the Paleocene-Eocene Thermal Maximum (PETM) was most severe at low latitudes, with sea surface temperatures at some localities exceeding the 35° C at which marine organisms experience heat stress. Relatively few equivalent terrestrial sections have been identified, and the response of land plants to this extreme heat is still poorly understood. Here, we present a new PETM record from the peak ring of the Chicxulub impact crater that has been identified based on nannofossil biostratigraphy, an acme of the dinoflagellate genus *Apectodinium*, and a negative carbon isotope excursion. Geochemical and microfossil proxies show that the PETM is marked by elevated TEX$_{86}^{H}$-based sea surface temperatures (SSTs) averaging ~37.8 °C, an increase in terrestrial input, surface productivity, salinity stratification, and bottom water anoxia, with biomarkers for green and purple sulfur bacteria indicative of photic zone euxinia in the early part of the event. Pollen and plants spores in this core provide the first PETM floral

assemblage described from México, Central America, and the northern Caribbean. The source area was a diverse coastal
40   shrubby tropical forest, with a remarkably high abundance of fungal spores indicating humid conditions. Thus, while
seafloor anoxia devastated the benthic marine biota, and dinoflagellate assemblages were heat-stressed, the terrestrial plant
ecosystem thrived.

1 Introduction and geologic setting

The Paleocene-Eocene Thermal Maximum (PETM) was a period of global warming associated with ocean acidification, an
45   intensified hydrological cycle, reductions in marine dissolved oxygen concentrations, eustatic sea level rise, and major
ecological shifts (e.g., Zachos et al., 2003; Gingerich 2006; Dickson et al., 2014; Sluijs et al., 2014; Carmichael et al., 2017).
Recent age estimates place the PETM at approximately 55.93-55.71 Ma (Westerhold et al. 2017; Hollis et al. 2019). The
onset of the PETM is marked by a global negative carbon isotope excursion (CIE) (Dickens et al. 1997; Gradstein et al.
2012). Possible sources of this isotopically light carbon include methane clathrates, combustion of organic matter,
50   thermogenic methane, desiccation of epicontinental seas, and organic matter released from permafrost (McInerney and
Wing, 2011). Sea surface temperature (SST) during the PETM in some low-latitude regions exceeded 35 °C, resulting in
heat stress for eukaryotic plankton (e.g., Frieling et al., 2018). In contrast, the few existing PETM records of low-latitude
terrestrial plant assemblages indicate an increase in diversity (e.g., Jaramillo et al., 2010; Srivastava and Prasad, 2015;
Prasad et al., 2018). Here, we established a new multiproxy record of the response of marine and terrestrial biota to the
55   PETM in the western Caribbean/Gulf of Mexico at International Ocean Discovery Program (IODP) Expedition 364 Site
M0077. This includes the first published pollen and spore PETM assemblage from tropical North America (Smith et al.,
2019, 2020). These data allow us to determine the extent of marine and terrestrial heat stress from the understudied region
and determine how they compare with other PETM sections.

        Site M0077 is located on the peak ring of the Chicxulub impact crater in the Yucatán Peninsula, México (Fig. 1)
60   (Morgan et al., 2017). The crater was a marine depositional basin in the Paleogene, with mainly pelagic and outer-platform
sediment deposition (Lefticariu et al., 2006). Immediately after impact, some of the rim may have been subaerially emergent
(Morgan et al., 1997), but, if so, would have been quickly eroded. During the PETM, only isolated areas of the crater rim
were still emergent, given the existence of an embayment into the crater to the north and northwest (Gulick et al., 2008).
Although PETM records from the Gulf of Mexico are scarce, another site in the Chicxulub crater, the Yaxcopoil-1 (Yax-1)
65   core, contains a PETM section identified by a negative carbon isotope excursion, deposited during a period of maximum
flooding (Whalen et al., 2013) (Fig. 1). The PETM has also been identified on the Mississippi paleoshelf (Fig. 1), where
evidence indicates increased TEX$_{86}^{H}$-based SSTs, photic zone euxinia, and sea level rise (Sluijs et al., 2014).

2 Methods

Quantitative palynological abundances are expressed in terms of specimens per gram, using a *Lycopodium* spike. Species
70 counts, descriptions, and paleoecological interpretations can be found in Smith et al. (2019, 2020). The D/S ratio between
dinoflagellate cysts and pollen/plant spores is described in Warny et al. (2003). The degree of bioturbation has been
quantified using the Bioturbation Index (BI) (Taylor and Goldring, 1993). Samples for $\delta^{15}N$ and $\delta^{13}C_{TOC}$ (n = 51) analyses
were prepared by acidifying approximately 0.5 g subsamples of powdered material with an excess of 1 M HCl. The acid-
insoluble residues were neutralized, freeze-dried and analyzed for their carbon and nitrogen contents as well as stable isotope
75 compositions using a Costech Elemental Analyzer (ECS 4010) and a Delta+XP mass spectrometer. Typical instrumental
precision of the isotope measurements is <0.2‰. Clay mineral assemblages were identified by X-ray diffraction on oriented
mounts of non-calcareous clay-sized particles (<2 μm). SSTs based on isoprenoidal glyceroldialkylglyceroltetraethers
(isoGDGTs) (Schouten et al. 2002) were reconstructed using the TEX_{86}^H calibration of Kim et al. (2010). Additional methods
are provided as supplementary materials along with all data.

80 3 Results

IODP drilling at Site M0077 recovered Paleocene to early Eocene post-impact sedimentary rocks between 617.33-505.70
meters below seafloor (mbsf). The PETM section (607.27-607.06 mbsf) is a laminated black to dark gray shale, separated
from an upper Paleocene carbonate hardground by an unconformity, and grading upwards into a burrowed lower Eocene
packstone (Fig. 2). Bioturbation is absent to minimal in the PETM, with rare *Chondrites* ichnofossils, except at the top of the
85 interval (607.11-607.06 mbsf) where *Planolites* burrows are observed, infilled with sediment from the overlying packstone.
The clay mineral assemblages are dominated by R0 random illite/smectite mixed layers (up to 90%), and also contains traces
of chlorite, illite, and palygorskite. The latter is rare in the upper Paleocene, and increases in abundance through the PETM,
reaching a peak of 5% relative abundance at 607.08 mbsf. The PETM interval is characterized by a marked increase in
magnetic susceptibility (χ), anhysteretic remanent magnetization (ARM), and isothermal remanent magnetization (IRM).
90 The average values increase by a factor of 15.7, 5.8, and 12.4 for χ, ARM, and IRM, respectively, compared to the average
values over the analyzed pre-PETM interval (607.67-607.27 mbsf) (see supplementary materials).

Total organic carbon (TOC) is low above and below the PETM (Fig. 2), with high concentrations (>6% rock
weight) in the upper PETM section. Total organic carbon/total nitrogen (TOC/TN) ratios range from 0.6 to 6.8 in the upper
Paleocene, with higher values averaging 10.7 in the PETM section. TOC/TN values in the post-PETM section range from
95 1.4 to 4.7. $\delta^{13}C_{TOC}$ ranges from -27.5‰ to -25.8‰ in the upper Paleocene and is -28.4‰ at the base of the PETM section,
generally becoming more negative upsection through the PETM, with the most depleted value of -30.1‰ in the upper PETM
(607.12 mbsf). Above 607.07 mbsf, $\delta^{13}C_{TOC}$ values become more positive, then stabilize at -27.5‰ at 607.03 mbsf. $\delta^{15}N$
ranges from 1.0‰ to 3.7‰ in the upper Paleocene and is 5.3‰ at the base of the PETM section, with more depleted values
through the PETM, reaching a minimum of -2.0‰ at 607.21 mbsf. The PETM $\delta^{15}N$ record is marked by two negative

100   excursions with values below 0‰, separated by a brief interval of positive $\delta^{15}N$ values between 607.17-607.13 mbsf. Above 607.10 mbsf, $\delta^{15}N$ values become more positive, with a value of 0.9‰ at 607.02 mbsf (Fig. 2).

TEX_{86}^{H}-based SSTs and other biomarkers were difficult to retrieve in the late Paleocene due to low organic matter content (TOC values often <0.1%), but a single sample at 607.33 mbsf yielded a TEX_{86}^{H}-based SST of 34.0 °C. In the PETM, TEX_{86}^{H}-based SSTs ranged from 37.4-38.0 °C, averaging 37.8 °C. Just above the PETM section, at 607.05 mbsf, the

105   TEX_{86}^{H}-based SST was 37.9 °C, followed by a decrease in SSTs to 37.1 °C and 37.3 °C at 606.87 and 606.72 mbsf, respectively (Fig. 2). The branched isoprenoid tetraether index (BIT) in the uppermost Paleocene (607.33 mbsf) is 0.16, while values of this index average 0.01 in the PETM section. In the post-PETM section BIT values are slightly higher and range from 0.04 to 0.05. Green and purple sulfur bacteria biomarkers (chlorobactane, okenane, and isorenieratane) reach their highest concentrations near the bottom of the PETM section, with low concentrations through the rest of the event (Fig.

110   2). Nannofossil abundances decrease through the PETM section and become rare in the post-PETM section. Foraminifera at Site M0077 are frequent to abundant in the upper Paleocene section but are absent to very rare in the PETM section, with evidence of reworking. Dinosterane concentrations are relatively high in the upper Paleocene and lower PETM section, with decreased abundance in the PETM and post-PETM sections. Organic-walled microfossils are absent to rare in the Paleocene. Dinoflagellate cyst concentrations peak at 607.26 mbsf, with a decreasing trend through the rest of the PETM (Fig. 2).

115   Relative abundances of *Apectodinium* are highest at 607.26 mbsf, and decrease through the PETM, while the highest relative abundances of Goniodomidae are found just above the event. Pollen and fungal spore concentrations peak in the middle PETM section (Fig. 2). The fungal assemblage is dominated by *Nigrospora*-types, which are common leaf endophytes on a variety of substrates, including soil, and are commonly airborne (Wang et al. 2017). The pollen and plant spore assemblage is dominated by *Malvacipollis* (Euphorbiaceae), *Ulmipollenites* (Ulmaceae), *Bohlensipollis* (Eleagnaceae), and angiosperm

120   pollen of unknown lower botanical affinity, with rare gymnosperm pollen and lower plant spores.

4 Discussion

4.1 Stratigraphy and sedimentology

The uppermost Paleocene, underlying the PETM interval, is characterized by two significant disconformities. The lower disconformity is atop a 6-8 cm thick gray claystone (607.66 mbsf), interpreted to be a bentonite, with an erosionally scoured

125   upper surface. It is overlain by a 7 cm thick carbonate rudstone that grades upward into a 22 cm thick packstone. The rudstone contains claystone and carbonate lithoclasts up two 2 cm in diameter, foraminifera, and lime mud, and grades into a light gray foraminiferal packstone with wispy stylolitic laminae. The packstone is overlain by a 4.5 cm thick gray claystone. Both the contact between the packstone and claystone and the claystone itself are burrowed and one burrow is infilled by material from the overlying facies. The claystone is abruptly overlain by a carbonate grainstone with planktic and large

130   benthic foraminifera, red algae, ostracods, calcispheres, and black and gray carbonate lithoclasts. The top of this unit (607.27 mbsf) is a hardground and disconformity with about 1 cm of relief. The lower contact of the grainstone with the underlying

claystone (607.32 mbsf) also appears to be unconformable, but no biozones are missing, so it may represent a diastem rather than a significant hiatus.

The PETM interval is about 21 cm thick. It has a sharp basal contact that drapes over the relief atop the underlying hardground. The PETM interval consists of dark gray to black shale that is laminated at the mm scale. The base of the interval is slightly lighter colored gray shale and contains clay, organic matter, sand-sized carbonate lithoclasts and foraminifera eroded from the underlying unit, as well as rare green grains and spherules that appear to be altered impact glass. The remainder of the PETM interval consists of mm-scale laminae that are usually dark gray at their base and black at the top and contain quartz, muscovite, rare plagioclase silt grains, and rare calcispheres. Laminae are commonly defined at their base by quartz and muscovite silt and grade upward into clay and organic-rich shale. The uppermost PETM shale is bioturbated, with burrows infilled with material from the overlying carbonate packstone. The interval directly overlying the PETM also contains abundant reworked material, including several pebble-sized clasts of limestone which appear to contain Cretaceous foraminifera.

The fine-grained nature and lack of sedimentary structures indicating current deposition indicate that the PETM interval was deposited in relatively deep, quiet water with sediments largely settling from suspension. The laminated black shale points toward low oxygen conditions. However, the trace fossil assemblage implies that anoxia and/or euxinia were likely intermittent. Water depths for Site M0077 during most of the Paleocene were on the order of 600-700 m (Lowery et al., 2018) but the facies immediately underlying and overlying the PETM interval contain numerous grains from shallow water environments, like larger benthic foraminifera and red algae which indicate either relatively shallow water in the crater or extensive reworking from the crater margin. Assigning a water depth for the PETM interval is complicated by the complete lack of obviously *in situ* depth-sensitive benthic foraminifera that could provide such insight. However, the presence of deeper-dwelling planktic foraminifera such as *Subbotina* spp. and *Globanomalina pseudomenardii*, which occupied a thermocline habitat (e.g., Aze et al., 2011) indicate that the water was at least deep enough for the establishment of stratification. The PETM is globally characterized by an eustatic sea level rise (Sluijs et al., 2008) so water depths were likely somewhat deeper during the PETM than during the times when the units above and below were deposited. This suggests that the shallow water fossils in the PETM interval were reworked from the crater rim, consistent with the interpretation of Whalen et al. (2013) that a roughly PETM age reworked deposit in the Yaxcopoil-1 core spread across the crater.

The PETM age of the shale interval at Site M0077 (607.27-607.06 mbsf) has been confirmed by a negative carbon isotope excursion (CIE) and biostratigraphy. The earliest nannofossil PETM sample, at 607.25 mbsf, contains *Discoaster salisburgensis* var. *anartios*, a characteristic PETM excursion taxon (Bralower and Self-Trail, 2016). The global negative CIE is also observed at Site M0077 (Fig. 2). In complete records of the PETM, the peak of the negative CIE and highest temperatures are observed within the first ~20 ky of the event, followed by a gradual recovery to more positive $\delta^{13}C_{TOC}$ values and lower SSTs (Hollis et al., 2019). However, at Site M0077, the most depleted $\delta^{13}C_{TOC}$ values are found in the upper PETM section. The onset and peak of the PETM CIE are missing due to erosion or non-deposition. The abrupt shift to more

positive $\delta^{13}C_{TOC}$ values at 607.06 mbsf suggests that the later PETM body and recovery is also missing, with another unconformity at the top of the PETM section. The trend towards more negative $\delta^{13}C_{TOC}$ values in the PETM can be explained as the result of an increasing contribution of terrestrial organic matter. This explanation is consistent with the palynological D/S ratio, which shows the highest relative abundance of terrestrial versus marine palynomorphs at approximately the same

170   depth as the most negative $\delta^{13}C_{TOC}$ values (Fig. 2). Increasing TOC/TN ratios are also consistent with a higher input of terrestrial organic matter through the PETM (Burdige, 2006). Lithologically, the PETM section is clearly distinguished from the Paleocene section by an abrupt switch from carbonate to siliciclastic clay deposition, and an abrupt increase in detrital input, as indicated by increased magnetic parameters.

4.2 PETM environmental change

175   SSTs were estimated using the relative abundance of thaumarchaeotal isoGDGTs. We here used the $TEX_{86}{}^{H}$ and the SST-calibration of Kim et al. (2010) developed for the determination of SSTs in (sub)tropical oceans and low latitude settings. The uncertainties associated with TEX_{86} estimates of SSTs exceeding the present-day SST maximum of 27-29 °C have been addressed for Cretaceous (O´Brian et al., 2017) and Tertiary (Frieling et al., 2017) strata. These authors conclude that during hyperthermals $TEX_{86}{}^{H}$ delivers reliable SST reconstructions, whereby an upper limit of the calibration has been proposed to

180   occur at 38.6 °C (Tierney and Tingley, 2014; O`Brian et al., 2017). In previous studies an impact of terrigenic derived GDGTs on the TEX_{86} proxy has been observed, in cases when the BIT index exceeded values of 0.3 (Weijers et al., 2006) or 0.4 (Schouten et al., 2013). In this study all BIT values remained below 0.2, indicating that inputs of terrigenic isoGDGTs do not compromise the $TEX_{86}{}^{H}$ paleothermometer

        $TEX_{86}{}^{H}$-based SSTs increased by ~4 °C between the late Paleocene and PETM (Fig. 2), with average PETM SSTs

185   of 37.8 °C, similar to values observed in the eastern equatorial Atlantic (Frieling et al., 2018) and the Dahomey Basin, western Africa (Frieling et al., 2017), and ~3 °C higher than those observed in the Harrell Core (Sluijs et al., 2014). SSTs decrease to 37.1 and 37.3 °C in the post-PETM section at 606.87 and 606.72 mbsf, respectively. The temperature increase from the late Paleocene to PETM section is consistent with estimates of a 4-5 °C global mean surface temperature anomaly for the PETM (Dunkley Jones et al., 2013). Frieling et al. (2017), investigating a tropical marine PETM record from Nigeria,

190   estimated latest Paleocene SSTs of 32-34 °C, with average PETM SSTs of ~36 °C.

        Several lines of evidence indicate increased terrestrial input during the PETM, including increased concentrations of terrestrial palynomorphs, increased D/S and TOC/TN ratios, and an increase in detrital ferromagnetic minerals. Theoretically, this increase in terrestrial input could be the result of a relative sea level fall, but this would not be consistent with an interpreted PETM sea level rise in the Gulf of Mexico and globally (Sluijs et al., 2014). Instead, the increase in

195   terrestrial input is interpreted to result from an intensified hydrological cycle during the PETM, as noted in other studies (e.g., Crouch et al., 2003; Bowen et al., 2004; Schmitz and Pujalte, 2007; Handley et al., 2012). The exceptionally high abundance of fungal spores in the PETM section suggests that increased humidity and terrestrial weathering resulted in greater detrital and nutrient input to Site M0077. BIT index values, which have been used as a proxy for terrestrial organic

matter in sediments (Hopmans et al., 2004; Weijers et al., 2006), are higher in the late Paleocene than in the PETM section
200   (Fig. 2). Low BIT values in samples from the PETM section may indicate a source of terrestrial organic matter lean in soil
microbial matter (Huguet et al., 2007; Schouten et al., 2013), possibly from low-lying carbonate terrain to the south (Fig. 1)
and/or an increased productivity of Thaumarchaeota.

     The relative abundance of the clay mineral palygorskite increases through the PETM section. Higher abundances of
palygorskite in other PETM sections have been interpreted as evidence for increased aridity (Carmichael et al., 2017), as
205   palygorskite commonly forms in coastal marine environments where continental alkaline waters are concentrated by
evaporation (Bolle and Adatte, 2001). At Site M0077, the palygorskite may have originally formed in hypersaline lagoonal
environments similar to other Eocene-Oligocene palygorskite deposits in the Yucatán Peninsula (de Pablo Galán, 1996). The
increase in relative abundance of palygorskite through the PETM section may therefore be the result of increased fluvial
transport of sediments to Site M0077 from lagoonal environments to the south, rather than the result of increased aridity.

210   The near absence of bioturbation in the PETM section, with preserved sedimentary laminations and high TOC, is
consistent with bottom water anoxia through much of the PETM, and sulfur bacteria biomarkers are indicative of photic zone
euxinia (e.g., Summons and Powell, 1987; Grice et al., 2005; Sluijs et al., 2014) in the earlier PETM record. Depleted $\delta^{15}N$
values, similar to those observed during ocean anoxic events (e.g., Jenkyns, 2010) can be explained by upwelling of
ammonium from anoxic deep waters during periods of high nutrient availability (e.g., Higgins et al., 2012), or increased
215   cyanobacterial N_2 fixation (e.g., Bauersachs et al., 2009). The transient positive $\delta^{15}N$ excursion in the middle of the PETM
section at Site M0077 (Fig. 2) is similar to the $\delta^{15}N$ PETM record of Junium et al. (2018) from the northern Peri-Tethys
seaway, with depleted $\delta^{15}N$ in the top and bottom of the PETM section, separated by an interval of more enriched $\delta^{15}N$,
which they interpreted to result from a more oxic, less stratified water column, possibly due to reduced freshwater influx.

4.3 Implications for life and climate

220   In the Paleocene interval at Site M0077, carbonate deposition dominates, and palynomorphs are nearly absent, probably due
to poor preservation of organic material (Lowery et al., 2018). Low values of TOC/TN (<4) observed in the Paleocene
section are also an indication of degradation of organic matter, with the breakdown of nitrogenous compounds to ammonia
and organic carbon escape via CO_2 release during oxidation (Müller, 1977; Meyers and Shaw, 1996). The late Paleocene
palynological samples in the carbonate hardground represent the oldest dinoflagellate assemblages observed in abundances
225   sufficient for paleoecological interpretation. Dinoflagellate cyst and dinosterane concentrations peak in the early PETM
interval, then decrease through the rest of the PETM, suggesting that the extreme warmth during the PETM resulted in heat-
stressed plankton within the Chicxulub impact crater, similar to the eastern equatorial Atlantic (Frieling et al., 2018).
Dinoflagellate assemblages record a peak in *Apectodinium* relative abundance in the bottom PETM section, with a
decreasing trend through the PETM. Increases in the relative abundance of Goniodomidae through the PETM likely indicate
230   an intensification in salinity stratification (e.g., Frieling and Sluijs, 2018). The PETM nannoplankton assemblage also
contains malformed *Discoaster* specimens, which may represent ecophenotypes that migrated to a deep photic zone refuge to

escape inhospitable SSTs and became malformed due to increased organic matter remineralization and calcite undersaturation (Bralower and Self-Trail, 2016).

A notable acme of fungal spores occurs in the middle part of the PETM and suggests humid forest and grassland ecosystems in the source area of the terrestrial palynomorphs. The PETM pollen and plant spore assemblage is broadly similar to later Ypresian assemblages observed higher in the core, with angiosperm pollen dominant and rare lower plant spores and gymnosperm pollen. The main pollen source area is interpreted as a lowland tropical forest and shrubland (Smith et al., 2019, 2020). Low abundances of grass pollen (*Monoporopollenites annulatus*) in the PETM suggest a minor grasslands component of the flora. Pollen with affinity to the Pinopsida and Ulmaceae may represent a contribution from more upland pollen source areas, based on their modern distributions in México and Central America. High concentrations of pollen in two PETM samples argue for a proximal pollen source area from low elevation carbonate terrain in the Yucatán Peninsula, consistent with modeled prevailing surface currents and summer wind fields from the south (Fig. 2) (Winguth et al., 2010). Globally, plant floras indicate shifts in ranges and relative abundances with low rates of extinction (Wing and Currano, 2013). These shifts are broadly indicative of warming during the PETM. Although plant assemblages in midlatitude continental interiors suggest drying during the PETM (e.g., Wing et al., 2005), PETM floral records from tropical South America (Jaramillo et al., 2010) and India (e.g., Prasad et al., 2018) suggest high levels of precipitation, while in tropical East Africa (Handley et al., 2012) evidence suggests a decrease in overall humidity but an increase in the intensity of precipitation events. The proxy data from Site M0077 indicates increased temperature and humidity in the Yucatán Peninsula during the PETM, resulting in increased terrestrial input.

5. Conclusions

The PETM in the Chicxulub impact crater was a time of extremely high SSTs (~37.8 °C), increased terrestrial input, high surface productivity, water column stratification, and bottom water hypoxia/anoxia, with evidence for photic zone euxinia in the bottom section. The observed increase in terrestrial input is likely the result of increased weathering and fluvial discharge due to moist, hyperthermal conditions. This explanation is consistent with global evidence of sea level rise during the PETM. Seafloor anoxia decimated the marine benthos during the PETM, while high SSTs caused heat stress in the dinoflagellate and likely other phytoplankton assemblages. In contrast, the pollen and spore assemblage indicates the presence of a proximal humid landmass with a diverse tropical shrubby forest, which produced relatively high abundances of Euphorbiaceae pollen. These results, in combination with previously described tropical PETM floral assemblages (Jaramillo et al. 2010; Srivastava and Prasad, 2015; Prasad et al., 2018), demonstrate that tropical vegetation was highly resilient to hyperthermal conditions.

Data availability

All data and supplementary methods are included as supplementary materials.

Team list (IODP Expedition 364 Scientists)

Joanna Morgan [Department of Earth Science and Engineering, Imperial College London, UK], Sean P.S. Gulick
265 [Department of Geological Sciences, Jackson School of Geosciences, University of Texas at Austin, Austin, TX 78712, USA; Institute for Geophysics, Jackson School of Geosciences, University of Texas at Austin, Austin, TX 78712, USA], Claire Mellett [British Geological Survey, The Lyell Center, UK], Johanna Lofi [CNRS, Aix-Marseille Univ, IRD, Coll France; INRAE, CEREGE, Aix-en-Provence, France], Elise Chenot [GeoRessources, Université de Lorraine, CNRS, France], Gail Christeson [Institute for Geophysics, Jackson School of Geosciences, University of Texas at Austin, Austin,
270 TX 78712, USA], Phillippe Clayes [Analytical, Environmental, and Geo-Chemistry, Vrije Universiteit Brussel, Belgium], Charles Cockell [Center for Astrobiology, School of Physics and Astronomy, University of Edinburgh, UK], Marco Coolen [Department of Chemistry, Western Australian Organic & Isotope Geochemistry Centre (WA-OIGC), Curtin University, Australia], Ludovic Ferrière [Natural History Museum, Austria], Catalina Gebhardt [Alfred Wegener Institute Helmholtz Centre of Polar and Marine Research, Germany], Kazuhisa Goto [International Research Institute of Disaster Science,
275 Tohoku University, Japan], Heather Jones [Department of Geosciences, Pennsylvania State University, University Park, PA 16801, USA], David Kring [Lunar and Planetary Institute, Houston, TX 77058, USA], Christopher Lowery [Department of Geological Sciences, Jackson School of Geosciences, University of Texas at Austin, TX 78712, USA], Rubén Ocampo-Torres [Groupe de Physico-Chimie de l'Atmosphère, L'Institut de chimie et procédés pour l'énergie, l'environnement et la santé (ICPEES), France], Ligia Perez-Cruz [Instituto de Geofísica, Universidad Nacional Autónoma De México, México],
280 Annemarie E. Pickersgill [School of Geographical and Earth Sciences, University of Glasgow, UK], Michael Poelchau [Department of Geology, University of Freiburg, Germany], Auriol Rae [Department of Earth Science and Engineering, Imperial College London, UK], Cornelia Rasmussen [Institute for Geophysics, Jackson School of Geosciences, University of Texas at Austin, USA], Mario Rebolledo-Vieyra [Unidad de Ciencias del Agua, Centro de Investigación Científica de Yucatán, A.C., México], Ulrich Riller [Institut für Geologie, Universität Hamburg, Germany], Honami Sato [Japan Agency
285 for Marine-Earth Science and Technology, Japan], Jan Smit [Faculty of Earth and Life Sciences FALW, Vrije Universiteit Amsterdam, Netherlands], Sonia Tikoo [Earth and Planetary Sciences, Rutgers University, New Brunswick, NJ 08854, USA], Naotaka Tomioka [Kochi Institute for Core Sample Research, Japan Agency for Marine-Earth Science and Technology, Japan], Michael Whalen [Department of Geosciences, University of Alaska Fairbanks, Fairbanks, AK 99775, USA], Axel Wittmann [LeRoy Eyring Center for Solid State Science, Arizona State University, AZ 85281, USA], Kosei
290 Yamaguchi [Department of Chemistry, Toho University, Japan], Long Xiao [School of Earth Sciences, Planetary Science Institute, China University of Geosciences (Wuhan), China], William Zylberman [CNRS, L'Institut de recherche pour le développement, Coll France, Aix Marseille University, France].

Author contributions

VS led the writing and organization of the manuscript. VS, SW, NNO, and JMO analyzed the terrestrial palynology. JV
295 analyzed the dinoflagellate assemblages. KG, BS, TB, and LS provided biomarker data and interpretation. MTW provided
carbon and nitrogen isotopes and sedimentologic evaluation of the core. KO provided additional isotope and geochemical
data. IA, JAA, and CL researched the foraminiferal assemblages. EC provided clay mineralogy data. HJ provided
nannofossil data. FJR provided ichnological data. JG and FD provided magnetic data. SPG, TB, JL, JM, and other co-authors
assisted with conceptualization and writing of the manuscript.

300 **Competing interests**

The authors declare that they have no conflict of interest.

Acknowledgements

This research used samples and data provided by the International Ocean Discovery Program (IODP). Funding was provided
by the CENEX (Center for Excellence in Palynology) Endowed Chair Fund, a 2018 James M. and Thomas J.M. Schopf
305 Award Student Research Grant from the Paleontological Society, an ARC-Discovery grant (DP180100982) from the
Australian Research Council (ARC), a postgraduate award from Curtin University, IODP-France, the Research Foundation
Flanders (FWO grant 12Z6618N) and NERC grant NE/P005217/1. Thanks to Roger E. Summons and Xingqian Cui (MIT,
US) for MRM analyses.

References

310 Aze, T., Ezard, T. H., Purvis, A., Coxall, H. K., Stewart, D. R., Wade, B. S. and Pearson, P. N.: A phylogeny of Cenozoic
macroperforate planktonic foraminifera from fossil data, Biological Reviews, 86(4), 900–927,
https://doi.org/10.1111/j.1469-185X.2011.00178.x, 2011.

Bauersachs, T., Schouten, S., Compaoré, J., Wollenzien, U., Stal, L. J., and Sinninghe Damsté, J. S.: Nitrogen isotopic
fractionation associated with growth on dinitrogen gas and nitrate by cyanobacteria, Limnology and Oceanography, 54(4),
315 1403–1411, https://doi.org/10.4319/lo.2009.54.4.1403, 2009.

Bolle, M.-P. and Adatte, T.: Palaeocene-early Eocene climatic evolution in the Tethyan realm: clay mineral evidence, Clay
Minerals, 36(2), 249–261, 2001.

Bowen, G. J., Beerling, D. J., Koch, P. L., Zachos, J. C., and Quattlebaum, T.: A humid climate state during the Palaeocene/
Eocene thermal maximum, Nature, 432(7016), 495, https://doi.org/10.1038/nature03115, 2004.

320   Bralower, T. J. and Self-Trail, J. M.: Nannoplankton malformation during the Paleocene-Eocene Thermal Maximum and its paleoecological and paleoceanographic significance, Paleoceanography, 31(10), 1423–1439, ttps://doi.org/10.1002/2016PA002980, 2016.

Burdige, D. J.: Geochemistry of marine sediments, Princeton University Press, Princeton, NJ., 2006.

Carmichael, M. J., Inglis, G. N., Badger, M. P., Naafs, B. D. A., Behrooz, L., Remmelzwaal, S., Monteiro, F. M., Rohrssen,

325   M., Farnsworth, A., and Buss, H. L.: Hydrological and associated biogeochemical consequences of rapid global warming during the Paleocene-Eocene Thermal Maximum, Global and Planetary Change, 157, 114–138, https://doi.org/10.1016/j.gloplacha.2017.07.014, 2017.

Crouch, E. M., Dickens, G. R., Brinkhuis, H., Aubry, M.-P., Hollis, C. J., Rogers, K. M., and Visscher, H.: The Apectodinium acme and terrestrial discharge during the Paleocene–Eocene thermal maximum: new palynological,

330   geochemical and calcareous nannoplankton observations at Tawanui, New Zealand, Palaeogeography, Palaeoclimatology, Palaeoecology, 194(4), 387–403, https://doi.org/10.1016/S0031-0182(03)00334-1, 2003.

Dickens, G. R., Castillo, M. M., and Walker, J. C.: A blast of gas in the latest Paleocene: Simulating first-order effects of massive dissociation of oceanic methane hydrate, Geology, 25(3), 259–262, https://doi.org/10.1130/0091-7613(1997)025<0259:ABOGIT>2.3.CO;2, 1997.

335   Dickson, A. J., Rees-Owen, R. L., März, C., Coe, A. L., Cohen, A. S., Pancost, R. D., Taylor, K., and Shcherbinina, E.: The spread of marine anoxia on the northern Tethys margin during the Paleocene-Eocene Thermal Maximum, Paleoceanography, 29(6), 471–488, https://doi.org/10.1002/2014PA002629, 2014.

Dunkley Jones, T., Lunt, D. J., Schmidt, D. N., Ridgwell, A., Sluijs, A., Valdes, P. J., and Maslin, M.: Climate model and proxy data constraints on ocean warming across the Paleocene–Eocene Thermal Maximum, Earth-Science Reviews, 125,

340   123–145, https://doi.org/10.1016/j.earscirev.2013.07.004, 2013.

Frieling, J. and Sluijs, A.: Towards quantitative environmental reconstructions from ancient non-analogue microfossil assemblages: Ecological preferences of Paleocene–Eocene dinoflagellates, Earth-Science Reviews, 185, 956–973, https://doi.org/10.1016/j.earscirev.2018.08.014, 2018.

Frieling, J., Gebhardt, H., Huber, M., Adekeye, O. A., Akande, S. O., Reichart, G.-J., Middelburg, J. J., Schouten, S., and

345   Sluijs, A.: Extreme warmth and heat-stressed plankton in the tropics during the Paleocene-Eocene Thermal Maximum, Science Advances, 3(3), e1600891, https://doi.org/10.1126/sciadv.1600891, 2017.

Frieling, J., Reichart, G.-J., Middelburg, J. J., Röhl, U., Westerhold, T., Bohaty, S. M., and Sluijs, A.: Tropical Atlantic climate and ecosystem regime shifts during the Paleocene–Eocene Thermal Maximum, Climate of the Past, 14(1), 39–55, https://doi.org/10.5194/cp-14-39-2018, 2018.

350   Gingerich, P. D.: Environment and evolution through the Paleocene–Eocene thermal maximum, Trends in Ecology & Evolution, 21(5), 246–253, https://doi.org/10.1016/j.tree.2006.03.006, 2006.

Gradstein, F. M., Ogg, J. G., Schmitz, M., and Ogg, G.: The Geologic Time Scale 2012, Elsevier, Amsterdam, Netherlands., 2012.

Grice, K., Cao, C., Love, G. D., Böttcher, M. E., Twitchett, R. J., Grosjean, E., Summons, R. E., Turgeon, S. C., Dunning,
355   W., and Jin, Y.: Photic zone euxinia during the Permian-Triassic superanoxic event, Science, 307(5710), 706–709,
https://doi.org/10.1126/science.1104323, 2005.

Gulick, S. P., Barton, P. J., Christeson, G. L., Morgan, J. V., McDonald, M., Mendoza-Cervantes, K., Pearson, Z. F.,
Surendra, A., Urrutia-Fucugauchi, J., and Vermeesch, P. M.: Importance of pre-impact crustal structure for the asymmetry of
the Chicxulub impact crater, Nature Geoscience, 1(2), 131–135, https://doi.org/10.1038/ngeo103, 2008.

360   Handley, L., O'Halloran, A., Pearson, P. N., Hawkins, E., Nicholas, C. J., Schouten, S., McMillan, I. K., and Pancost, R. D.:
Changes in the hydrological cycle in tropical East Africa during the Paleocene–Eocene Thermal Maximum,
Palaeogeography, Palaeoclimatology, Palaeoecology, 329, 10–21, https://doi.org/10.1016/j.palaeo.2012.02.002, 2012.

Hay, W. W. and Floegel, S.: New thoughts about the Cretaceous climate and oceans, Earth-Science Reviews, 115(4), 262–
272, https://doi.org/10.1016/j.earscirev.2012.09.008, 2012.

365   Higgins, M. B., Robinson, R. S., Husson, J. M., Carter, S. J., and Pearson, A.: Dominant eukaryotic export production during
ocean anoxic events reflects the importance of recycled NH4+, Proceedings of the National Academy of Sciences, 109(7),
2269–2274, https://doi.org/10.1073/pnas.1104313109, 2012.

Hollis, C. J., Dunkley Jones, T., Anagnostou, E., Bijl, P. K., Cramwinckel, M. J., Cui, Y., Dickens, G. R., Edgar, K. M.,
Eley, Y., and Evans, D.: The DeepMIP contribution to PMIP4: methodologies for selection, compilation and analysis of
370   latest Paleocene and early Eocene climate proxy data, incorporating version 0.1 of the DeepMIP database, Geoscientific
Model Development Discussions, 2019, 1–98, https://doi.org/10.5194/gmd-12-3149-2019, 2019.

Hopmans, E. C., Weijers, J. W., Schefuß, E., Herfort, L., Sinninghe Damsté, J. S. and Schouten, S.: A novel proxy for
terrestrial organic matter in sediments based on branched and isoprenoid tetraether lipids, Earth and Planetary Science
Letters, 224(1–2), 107–116, https://doi-org.libezp.lib.lsu.edu/10.1016/j.epsl.2004.05.012, 2004.

375   Huguet, C., Smittenberg, R. H., Boer, W., Sinninghe Damsté, J. S. and Schouten, S.: Twentieth century proxy records of
temperature and soil organic matter input in the Drammensfjord, southern Norway, Organic Geochemistry, 38(11), 1838–
1849, https://doi.org/10.1016/j.orggeochem.2007.06.015, 2007.

Jaramillo, C., Ochoa, D., Contreras, L., Pagani, M., Carvajal-Ortiz, H., Pratt, L. M., Krishnan, S., Cardona, A., Romero, M.,
and Quiroz, L.: Effects of rapid global warming at the Paleocene-Eocene boundary on neotropical vegetation, Science,
380   330(6006), 957–961, https://doi.org/10.1126/science.1193833, 2010.

Jenkyns, H. C.: Geochemistry of oceanic anoxic events, Geochemistry, Geophysics, Geosystems, 11(3), 1–30,
https://doi.org/10.1029/2009GC002788, 2010.

Junium, C. K., Dickson, A. J. and Uveges, B. T.: Perturbation to the nitrogen cycle during rapid Early Eocene global
warming, Nature Communications, 9(1), 3186, https://doi.org/10.1038/s41467-018-05486-w, 2018.

385   Kim, J.-H., Van der Meer, J., Schouten, S., Helmke, P., Willmott, V., Sangiorgi, F., Koç, N., Hopmans, E. C., and Sinninghe
Damsté, J. S.: New indices and calibrations derived from the distribution of crenarchaeal isoprenoid tetraether lipids:

Implications for past sea surface temperature reconstructions, Geochimica et Cosmochimica Acta, 74(16), 4639–4654, https://doi.org/10.1016/j.gca.2010.05.027, 2010.

Lefticariu, M., Perry, E. C., Ward, W. C. and Lefticariu, L.: Post-Chicxulub depositional and diagenetic history of the
390   northwestern Yucatan Peninsula, Mexico, Sedimentary Geology, 183(1), 51–69, https://doi.org/10.1016/j.sedgeo.2005.09.008, 2006.

Lowery, C. M., Bralower, T. J., Owens, J. D., Rodríguez-Tovar, F. J., Jones, H., Smit, J., Whalen, M. T., Claeys, P., Farley, K., and Gulick, S. P.: Rapid recovery of life at ground zero of the end-Cretaceous mass extinction, Nature, 558(7709), 288–291, https://doi.org/10.1038/s41586-018-0163-6, 2018.

395   McInerney, F. A. and Wing, S. L.: The Paleocene-Eocene Thermal Maximum: A perturbation of carbon cycle, climate, and biosphere with implications for the future, Annual Review of Earth and Planetary Sciences, 39, 489–516, https://doi.org/10.1146/annurev-earth-040610-133431, 2011.

Meyers, P. A. and Shaw, T. J.: Organic matter accumulation, sulfate reduction, and methanogenesis in Pliocene–Pleistocene turbidites on the Iberia Abyssal Plain, in Proceedings of the Ocean Drilling Program, Scientific Results, vol. 149, p. 705.,
400   1996.

Morgan, J., Warner, M., Brittan, J., Buffler, R., Camargo, A., Christeson, G., Denton, P., Hildebrand, A., Hobbs, R., Macintyre, H., Mackenzie, G., Maguire, P., Marin, L., Nakamura, Y., Pilkington, M., Sharpton, V., Snyder, D., Suarez, G., and Trejo, A.: Size and morphology of the Chicxulub impact crater, Nature, 390(6659), 472–476, https://doi.org/10.1038/37291, 1997.

405   Morgan, J.V., Gulick, S.P.S., Mellet, C.L., Green, S.L., and the Expedition 364 Scientists, 2017, Chicxulub: Drilling the K-Pg Impact Crater: Proceedings of the International Ocean Discovery Program, v. 364.

Müller, P. J.: CN ratios in Pacific deep-sea sediments: Effect of inorganic ammonium and organic nitrogen compounds sorbed by clays, Geochimica et Cosmochimica Acta, 41(6), 765–776, https://doi.org/10.1016/0016-7037(77)90047-3, 1977.

de Pablo Galán, L.: Palygorskite in eocene-oligocene lagoonal environment, Yucatan, Mexico, Revista Mexicana de
410   Ciencias Geológicas, 13(1), 6, 1996.

O'Brien, C. L., Robinson, S. A., Pancost, R. D., Sinninghe Damsté, J. S., Schouten, S., Lunt, D. J., Alsenz, H., Bornemann, A., Bottini, C. and Brassell, S. C.: Cretaceous sea-surface temperature evolution: Constraints from TEX$_{86}$ and planktonic foraminiferal oxygen isotopes, Earth-Science Reviews, 172, 224–247, https://doi.org/10.1016/j.earscirev.2017.07.012, 2017.

Prasad, V., Utescher, T., Sharma, A., Singh, I. B., Garg, R., Gogoi, B., Srivastava, J., Uddandam, P. R., and Joachimski, M.
415   M.: Low-latitude vegetation and climate dynamics at the Paleocene-Eocene transition–A study based on multiple proxies from the Jathang section in northeastern India, Palaeogeography, Palaeoclimatology, Palaeoecology, 497, 139–156, https://doi.org/10.1016/j.palaeo.2018.02.013, 2018.

Schmitz, B. and Pujalte, V.: Abrupt increase in seasonal extreme precipitation at the Paleocene-Eocene boundary, Geology, 35(3), 215–218, https://doi.org/10.1130/G23261A.1, 2007.

420   Schouten, S., Hopmans, E. C., Schefuß, E. and Sinninghe Damsté, J. S.: Distributional variations in marine crenarchaeotal membrane lipids: a new tool for reconstructing ancient sea water temperatures?, Earth and Planetary Science Letters, 204(1–2), 265–274, https://doi.org/10.1016/S0012-821X(02)00979-2, 2002.

Schouten, S., Hopmans, E. C. and Sinninghe Damsté, J. S.: The organic geochemistry of glycerol dialkyl glycerol tetraether lipids: a review, Organic geochemistry, 54, 19–61, https://doi-org.libezp.lib.lsu.edu/10.1016/j.orggeochem.2012.09.006,

425   2013.

Scotese, C. R. and Wright, N.: PALEOMAP paleodigital elevation models (PaleoDEMS) for the Phanerozoic, URL: https://www.earthbyte.org/paleodem-resource-scotese-and-wright-2018, 2018.

Sluijs, A., Brinkhuis, H., Crouch, E. M., John, C. M., Handley, L., Munsterman, D., Bohaty, S. M., Zachos, J. C., Reichart, G.-J. and Schouten, S.: Eustatic variations during the Paleocene-Eocene greenhouse world, Paleoceanography, 23(4), https://

430   doi.org/10.1029/2008PA001615, 2008.

Sluijs, A., Van Roij, L., Harrington, G. J., Schouten, S., Sessa, J. A., LeVay, L. J., Reichart, G.-J., and Slomp, C. P.: Warming, euxinia and sea level rise during the Paleocene–Eocene Thermal Maximum on the Gulf Coastal Plain: implications for ocean oxygenation and nutrient cycling, Climate of the Past, 10(4), 1421–1439, https://doi.org/10.5194/cp-10-1421-2014, 2014.

435   Smith, V., Warny, S., Jarzen, D., Demchuck, T., Vajda, V., and Expedition 364 Scientific Party: Paleocene-Eocene miospores from the Chicxulub impact crater, Mexico. Part 1: spores and gymnosperm pollen, Palynology, doi:10.1080/01916122.2019.1630860, 2019.

Smith, V., Warny, S., Jarzen, D., Demchuck, T., Vajda, V., and Gulick, S.: Paleocene-Eocene palynomorphs from the Chicxulub impact crater, Mexico. Part 2: angiosperm pollen, Palynology, doi:10.1080/01916122.2019.1705417, 2020.

440   Srivastava, J. and Prasad, V.: Effect of global warming on diversity pattern in Nypa mangroves across Paleocene–Eocene transition in the paleo-equatorial region of the Indian sub-continent, Palaeogeography, Palaeoclimatology, Palaeoecology, 429, 1–12, https://doi.org/10.1016/j.palaeo.2015.03.026, 2015.

Summons, R. E. and Powell, T. G.: Identification of aryl isoprenoids in source rocks and crude oils: biological markers for the green sulphur bacteria, Geochimica et Cosmochimica Acta, 51(3), 557–566, https://doi.org/10.1016/0016-

445   7037(87)90069-X, 1987.

Taylor, A. M. and Goldring, R.: Description and analysis of bioturbation and ichnofabric, Journal of the Geological Society, 150(1), 141–148, https://doi.org/10.1144/gsjgs.150.1.0141, 1993.

Tierney, J. E. and Tingley, M. P.: A Bayesian, spatially-varying calibration model for the TEX_{86} proxy, Geochimica et Cosmochimica Acta, 127, 83–106, https://doi.org/10.1016/j.gca.2013.11.026, 2014.

450   Wang, M., Liu, F., Crous, P. W. and Cai, L.: Phylogenetic reassessment of *Nigrospora*: ubiquitous endophytes, plant and human pathogens, Persoonia: Molecular Phylogeny and Evolution of Fungi, 39, 118, https://doi.org/10.3767/persoonia.2017.39.06, 2017.

Warny, S. A., Bart, P. J., and Suc, J.-P.: Timing and progression of climatic, tectonic and glacioeustatic influences on the Messinian Salinity Crisis, Palaeogeography, Palaeoclimatology, Palaeoecology, 202(1–2), 59–66,

455 https://doi.org/10.1016/S0031-0182(03)00615-1, 2003.

Weijers, J. W. H., Schouten, S., Spaargaren, O. C., Sinninghe Damsté, J. S.: Occurrence and distribution of tetraether membrane lipids in soils: Implications for the use of the TEX_{86} proxy and the BIT index. Org. Geochem. 37, 1680–1693, https://doi.org/10.1016/j.orggeochem.2006.07.018, 2006.

Westerhold, T., Röhl, U., Frederichs, T., Agnini, C., Raffi, I., Zachos, J. C., and Wilkens, R. H.: Astronomical calibration of

460 the Ypresian timescale: Implications for seafloor spreading rates and the chaotic behavior of the solar system, Climate of the Past, 13(9), 1129–1152, https://doi.org/10.5194/cp-13-1129-2017, 2017.

Whalen, M. T., Gulick, S. P. S., Pearson, Z. F., Norris, R. D., Perez-Cruz, L., and Urrutia-Fucugauchi, J.: Annealing the Chicxulub impact: Paleogene Yucatán carbonate slope development in the Chicxulub impact basin, Mexico, Deposits, Architecture, and Controls of Carbonate Margin, Slope and Basinal Settings. Special Publication-SEPM (Society for

465 Sedimentary Geology), 105, 282–304, https://doi.org/10.2110/sepmsp.105.04, 2013.

Wing, S. L. and Currano, E. D.: Plant response to a global greenhouse event 56 million years ago, American Journal of Botany, 100(7), 1234–1254, https://doi.org/10.3732/ajb.1200554, 2013.

Wing, S. L., Harrington, G. J., Smith, F. A., Bloch, J. I., Boyer, D. M., and Freeman, K. H.: Transient floral change and rapid global warming at the Paleocene-Eocene boundary, Science, 310(5750), 993–996, https://doi.org/10.1126/science.1116913,

470 2005.

Winguth, A., Shellito, C., Shields, C., and Winguth, C.: Climate Response at the Paleocene–Eocene Thermal Maximum to Greenhouse Gas Forcing—A Model Study with CCSM3, Journal of Climate, 23(10), 2562–2584, https://doi.org/10.1175/2009JCLI3113.1, 2010.

Zachos, J. C., Wara, M. W., Bohaty, S., Delaney, M. L., Petrizzo, M. R., Brill, A., Bralower, T. J., and Premoli-Silva, I.: A

475 transient rise in tropical sea surface temperature during the Paleocene-Eocene thermal maximum, Science, 302(5650), 1551–1554, https://doi.org/10.1126/science.1090110, 2003.

480

485
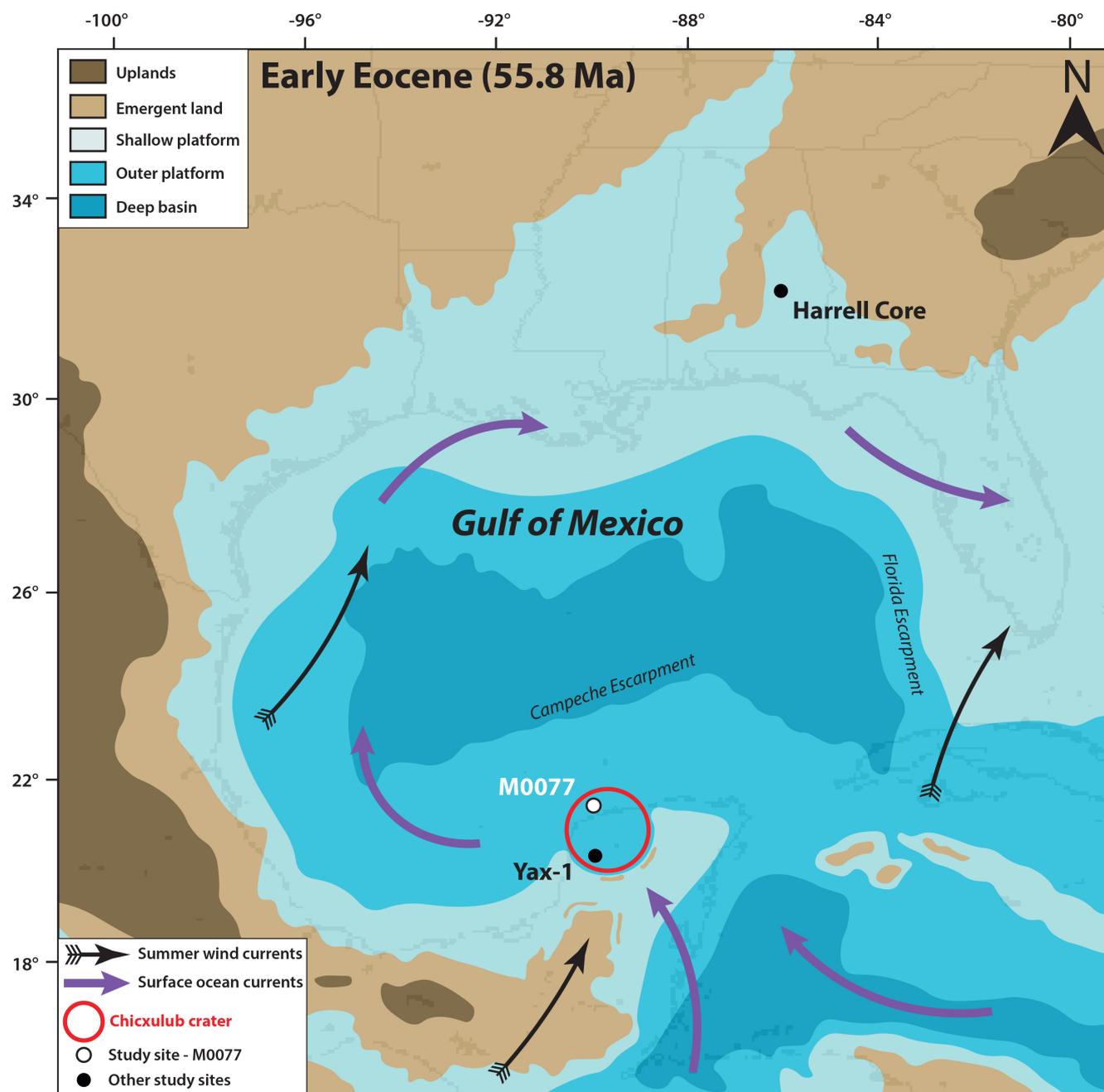
Figure 1. Paleocene-Eocene Thermal Maximum (55.8 Ma) paleogeography of the Gulf of Mexico and surrounding regions, modified from Scotese and Wright (2018), with locations of Site M0077 (IODP 364), Yax-1 (Whalen et al., 2013), and the Harrell Core in east-central Mississippi (Sluijs et al., 2014). The Harrell Core location has been adjusted to match the paleo-latitude/longitude at the PETM. Surface ocean currents and summer wind fields from Winguth et al. (2010).
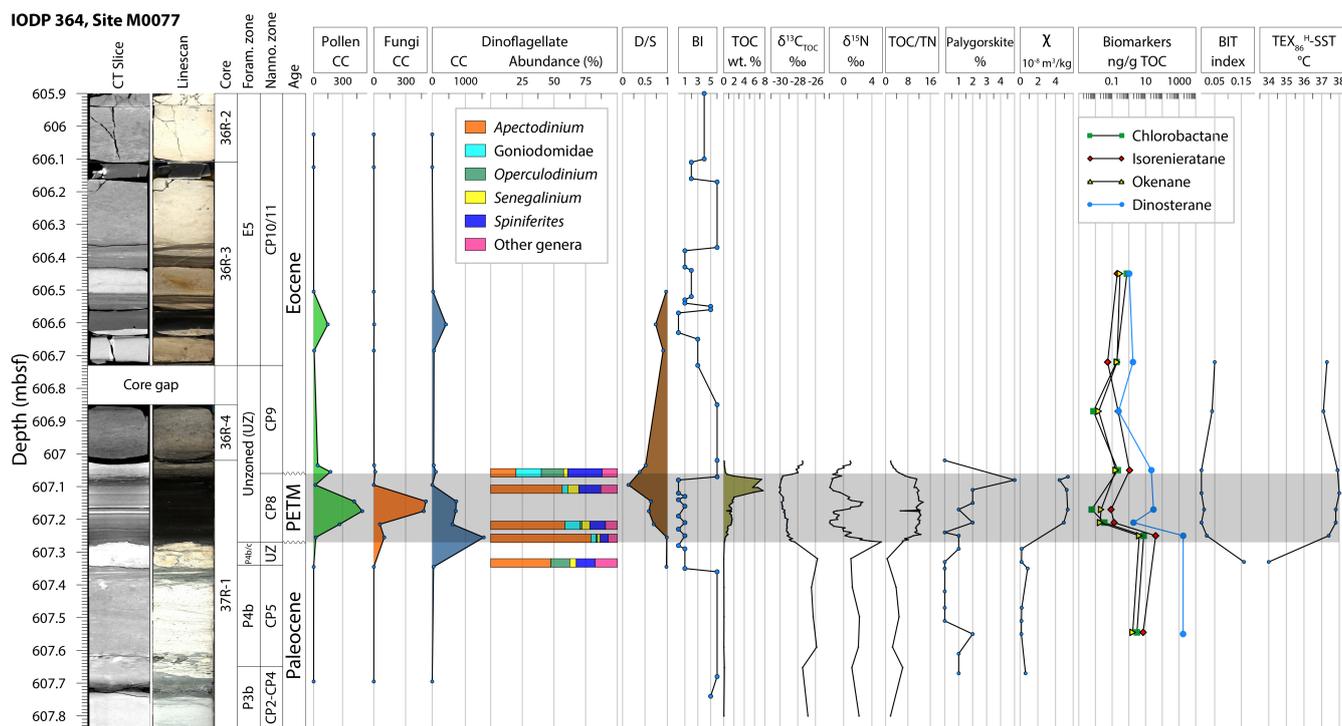
Figure 2. Stratigraphic column of Site M0077. Palynological concentrations (CC) are given as specimens/gram. $\delta^{15}N$ is reported relative to atmospheric N_2, $\delta^{13}C_{TOC}$ is reported relative to VPDB. BI=bioturbation index (Taylor and Goldring, 1993), CT=computed tomography, D/S=dinoflagellate cyst to pollen and plant spore ratio (Warny et al., 2003), TOC/TN=total organic carbon/total nitrogen, TOC=total organic carbon, χ=magnetic susceptibility.